Journal of Materials Chemistry C

Accepted Manuscript

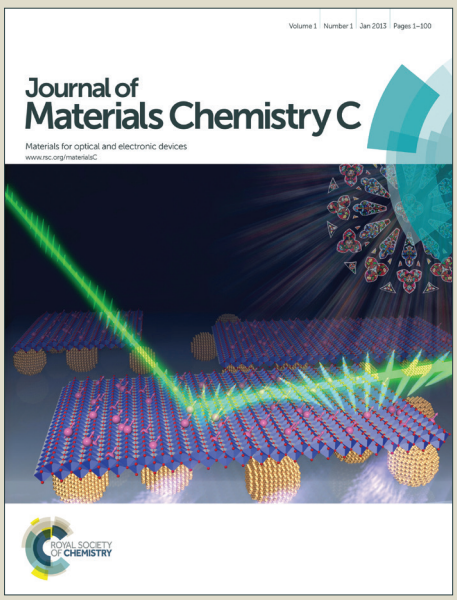

ROYAL SOCIETY OF CHEMISTRY

www.rsc.org/materialsC

Tunable Size and Sensitization of ZnO Nanoarrays as Electron Transport Layer for Enhancing Photocurrent of Photovoltaic Devices

Haiyan Fu[1], Licheng Tan[*1,2], Yueqin Shi[1], Yiwang Chen[1,2]

[1]School of Materials Science and Engineering/Institute of Polymers, Nanchang University, 999 Xuefu Avenue, Nanchang 330031, China; [2]Jiangxi Provincial Key Laboratory of New Energy Chemistry, College of Chemistry, Nanchang University, 999 Xuefu Avenue, Nanchang 330031, China

Abstract

Tunable size ZnO nanoarrays (NAs) sensitized with CdS, Ag_2S, CdS/Ag_2S quantum dots and solution processed 2-(2-(2-methoxyethoxy) ethoxy) ethyl undec-10-enyl malonate (EEMC) fullerenes have been developed as electron transport layer for improving polymer solar cells performance. ZnO NAs could provide direct and ordered electron channels for electron transportation, the optimized thickness of ZnO NAs was determined by means of contrast experiments with P3HT:$PC_{61}BM$ active layer. CdS, Ag_2S shell and CdS/Ag_2S double-shells could passivate the surface defects of ZnO NAs, increase the electron mobility and enhance light absorption. Besides, EEMC assist the infiltration of active layer into inorganic nanoarrays. Consequently, the performance of the inverted device based on thieno[3,4-b]-thiophene/benzodithiophene (PTB7):[6,6]-phenyl C_{71}-butyric acid methyl ester ($PC_{71}BM$) with ZnO/CdS/Ag_2S/EEMC core/multi-shells NAs as electron transport layer has been greatly improved to 7.7% with a high short-circuit current density of 17.9 mA/cm^2. Moreover, the fabrication process was low-cost and environment-friendly, which would be in favor of large-scale production of polymer solar cells.

* Corresponding author. Tel.: +86 791 83968703; fax: +86 791 83969561. *E-mail address*: tanlicheng@ncu.edu.cn (L. Tan).

Keywords: quantum dots; zinc oxide; nanoarrays; core/shells; polymer solar cells

Introduction

In the past decade, polymer solar cells (PSCs) have been received numerous attentions due to their low-cost, good film-forming, light weight, flexibility and large-area manufacturability.[1, 2] Recently, the power conversion efficiency (PCE) up to 10% has been reported owning to the improvement on the synthesis of high efficiency donors, optimized device structure, interfacial morphology control and processing optimization.[3-5]

Usually, the conventional and the inverted structure are the two main types of device architectures. The PSCs with conventional structure always suffer from the low-work-function metal cathode, oxidation of the air-sensitive, and the acidity and hygroscopicity of poly (3,4-ethylenedioxythiophene):poly(styrenesulfonate) (PEDOT:PSS), which can reduce the performance of the devices. To circumvent these problems, an inverted device structure is fabricated, where ITO is used as cathode to collect electrons, the high work-function metal (Ag or Au) is used as anode to collect holes, and n-type metal oxide (ZnO or TiOx,) is coated on ITO as electron transport layer (ETL). As a result, the device performance has been found to be improved significantly.[5]

Among the n-type metal oxides used in inverted cells, ZnO is a promising candidate due to its high electron mobility, physical and chemical stability and tunable optical properties.[6, 7] However, the major problems in using ZnO nanoparticle film as ETL are the poor spatial distribution and easy aggregation of the nanoparticles over a large area,[8, 9] the presence of defects with adsorbed oxygen,[10, 11] and limited interfacial

contact between active layer and ETL. Therefore, it is urgently desirable to develop a novel structure of ZnO ETL so as to realize high-efficiency inverted polymer solar cells. The use of vertically aligned one-dimensional (1-D) ZnO nanoarrays (ZnO NAs) instead of disordered ZnO nanoparticle film can provide an ideal architecture to obtain larger and more optimized interfacial area between active layer and ETL, and offer controllable and direct pathways for the transportation of electrons towards the collection electrode, subsequently, leading to a decrease in the probability of electron/hole recombination and enhancing the PCE.[12-14] As for its high electron mobility and easy production at low temperature,[15, 16] and enlarging interfacial area between active layer and ETL. And also ZnO NAs owe less junctions compared to ZnO nanoparticles, which would help optimizing the interpenetrating network of active layer to promote the charges transportation and collection at the corresponding electrode[17] In addition to being an electron transport layer, the n-type ZnO NAs in the proposed device configuration also acts as a second acceptor, resulting in an organic-inorganic contact which could pay a certain contribution of photocurrent.[18] Nevertheless, the thick ZnO NAs films possess a high concentration of deep level defects, and give rise to the trapping of electrons, which significantly influence the transportation of photogenerated charges towards the electrode.[13, 19, 20] To remedy the defects of ZnO NAs for interfacial engineering in PSCs, functional ligands (such as silanes, carboxylic acid, alkyl thiols and fullerene derivative[21-25]) are employed to passivate surface states of inorganic nanocrystals and reduce the electron depletion. Although organic interfacial modification could improve the compatibility between active layer and ZnO NAs layer, several primary issues should be considered, the relative low electrical conductivity (even insulating nature) and loosely connected network of organic ligands could resulting in a limited transportation of

photogenerated electron to the electrode.[26]

Inorganic modification of ZnO NAs surfaces is another promising method to boost the performance of PSCs. Lead sulfide (PbS),[27-29] lead selenide (PbSe) , cadmium sulfide (CdS) and cadmium selenide (CdSe)[30-32] quantum dots (QDs) have been demonstrated to enhance photocurrent in metal-oxide nanowire arrays. To better engineering the semiconductor sensitizer structure, quasi-quantum well structure of zinc selenide (ZnSe)/cadmium selenide (CdSe)/zinc selenide (ZnSe)[33] has been used to sensitize solar cells and a PCE of 6.2% is attained. Besides that, PbS/CdS QDs shells have been also employed to ameliorate titanium dioxide (TiO_2) nanorod arrays,[27] and all the devices have revealed much faster electrons transport and much lesser recombination. However, the overmuch use of toxic Cd and Pb compounds may be eventually terminated because of the increasingly acrimonious environmental requirement.[34] Silver sulfide (Ag_2S) is environmental friendly and stably exposing to the acid and moisture, as well as a near-infrared absorbed binary semiconductor with a narrow band gap of ~0.9 eV.[35] Zheng *et al*.[36] first reported the fabrication of P3HT:Ag_2S hybrid solar cells obtaining outstanding short-circuit current density (J_{sc}) around 20 $mA \cdot cm^{-2}$ and PCE of 2.04%.

Herein, in view of the high concentration surface defects of ZnO NAs, a narrow-band gap semiconductor Ag_2S was first applied to sensitize the ZnO NAs. Likewise, the CdS QDs,[37-39] as its high stability under irradiation, good controllability in the fabrication process and excellent optical properties have been utilized to sensitize ZnO NAs. Different shells were deposited on the top of ZnO NAs by a water-soluble and environment-friendly method, forming nanoarrays of the inner ZnO NAs core

with outer shell Ag_2S and CdS respectively, defined as ZnO/Ag_2S NAs (ZA NAs) and ZnO/CdS NAs (ZC NAs). And the thickness of corresponding NAs by controlling the hydrolysis time was primarily investigated. Taking multiple advantages (including the environment-friendly property of Ag_2S, good photo-electricity of CdS and solution processability of ZnO NAs) into consideration, the ZnO NAs core with multideck shells of CdS and Ag_2S simultaneously, named as ZnO/CdS/Ag_2S NAs (ZCA NAs) were successfully synthesized. Besides, a solution-processed small organic molecule 2-(2-(2-methoxyethoxy) ethoxy) ethyl undec-10-enyl malonate (EEMC) had been synthesized,[40] and the synthetic process and structure are shown in **Figure S1**, which can modify the inorganic surface defects and enhance the compatibility of organic active layer and inorganic nanoarrays for enhancing PCE.[41] The mutual effect between the interfacial compatilizer of solution-processed fullerenes and the electron acceptor fullerenes assisted the infiltration of active layer into inorganic nanoarrays, which would increase interface areas for enhancing the performance of PSCs devices. All fabrication processes were environment-friendly, which would be benefit for large scale and low cost production of polymer solar cells.

Results and Discussion

The synthesis process and structure of the device in this work are schematically illustrated in **Scheme 1**, and the detailed experiment and characterization sections are shown in **Supporting Information**. The ZnO NPs nucleation centers were spin-coated on ITO substrate, subsequently the ZnO NAs were formed via low temperature hydrothermal method and QDs shells were covered on ZnO NAs through a water-soluble and environment-friendly successive ion layer adsorption and reaction (SILAR).[42]

Figure 1 establishes the morphology images of ZnO NPs and ZnO NAs vertically aligned on the ITO substrate with different thickness by controlling the hydrolysis time. It could be estimated that ZnO NPs own a diameter of 5-10 nm**,** and it can be seen that the ZnO NAs are vertical and hexagonal, agreeing with previous reports.[23,36] With the hydrolysis time ranging from 0 min to 120 mins, the thickness of ZnO NAs remarkably changes from 39±5 nm to 222±10 nm, verified by the SEM and surface profilometer (AMBIOS TECHNOLOGY ltd. XP-2).The component of the nanoarrays has also been confirmed by X-ray photoelectron spectroscopy (XPS) measurements. The inset of **Figure 1** shows XPS spectra of Zn 2p and O 1s elements on surface of the nanoarrays, which could prove the formation of ZnO NAs. Furthermore, in **Figure 1**, high resolution transmission electron microscopy (HRTEM) presents lattice spacing of the nanoarrays is 0.52 nm in the <0001> direction, which is consistent with the known hexagonal wurtzite ZnO NAs.[29, 43] All the scanning electron microscopy (SEM) and transmission electron microscopy (TEM) analysis confirm that the ZnO NAs with an average diameter of 20-50 nm, an areal density of 300-400 nanoarrays/μm^2, and an average inter-nanoarrays spacing of 10-20 nm, which are coincided with the charge-separating of 10 nm length-scale for reducing the recombination of the electron-hole pairs.[44] And it is well known that the intermixed nanostructure can enlarge the interfacial area for electron transporting,[45, 46] but too thick ZnO NAs layer could lead to high concentration of surface defects and increasing charges recombination. Hence, the optimized thickness of ZnO NAs layer for PSCs would be discussed in below.

The photovoltaic performance of ZnO NAs/P3HT:$PC_{61}BM$ devices are summarized in

Figure 2 and **Table 1**. The short-circuit current density (J_{sc}), open circuit voltage (V_{oc}) and fill factor (FF) are all improved when hydrolysis time ranging from 0 to 20 mins (corresponding thickness from 39 nm to 60 nm). The optimized device based on 60 nm thickness of ZnO NAs layer achieves a PCE of 3.6% under AM 1.5 illuminsation (100 mW/cm^2), with J_{sc} of 9.68 mA/cm^2, V_{oc} of 0.58 V, FF of 63.7%. The vertical ZnO NAs as ETL lead to a larger interfacial contact comparing to ZnO NPs, and also provide direct, stable and fast pathways for the transportation of electrons and collection towards electrode.[13] The cross-section image (**Figure 1)** exhibits that the active layer immerse suitably into ZnO NAs, which provides a direct and stable pathway for the transportation of photogenerated electrons towards the collection electrode. Furthermore, the device reveals more light harvesting and enhanced J_{sc} by inserting an vertical aligned ZnO NAs optical spacer with appropriate thickness.[47] However, with the hydrolysis time increasing to 120 mins, a significantly decrease of J_{sc} (5.69 mA·cm^{-2}) and V_{oc} (0.45V) for ZnO NAs (222 nm) ETL is observed. Too thick ZnO NAs possess higher concentration surface defeats and resist the infiltration of active layer to some extent, thus resulting in poor interfacial contact and evident voids between ZnO NAs layer and active layer.[48] And also the too thick ZnO NAs would reduce the electron conductivity of the buffer layer.

As shown in **Figure 3,** all sensitized ZnO NAs (ZA NAs, ZC NAs and ZCA NAs) are vertically aligned on the ITO substrate, which are not remarkably altered comparing to ZnO NAs (**Figure 1**), and Ag_2S and CdS quantum dots can be fully covered onto the corresponding ZnO NAs (testified by the insert of XPS data, respectively). Cross-sectional SEM figure of ZCA NAs (**Figure 3)** reveals that Ag_2S and CdS quantum dots adsorb on the ZnO NAs together. TEM image (**Figure 3**) analysis

further confirms the original ZnO NAs have been turned into ZA NA s after Ag_2S deposition in agreement with the insert of XPS data, and Ag_2S shell with thickness of about 5 nm as quantum dots are in close proximity to the underlying nanoarrays. The X-ray diffraction (XRD) patterns (in **Figure S2**) of ZnO NAs and ZA NAs with different thickness of Ag_2S shell presents that ZnO NAs grow perfectly at the peak (002) of 34.4º, indicating the preferential growth along the <0001> direction[29] according with HRTEM (**Figure 1**), and the thick shell contains large quantum dots with a higher diffraction peak. The core/multi shells structure is a vertical configuration which might be optimal for their integration into different top contact electrode devices.[49] Cross-sectional SEM figure of ZCA NAs/PTB7:$PC_{71}BM$ after annealing treatment (**Figure 3**) shows that the active layer could be successfully permeated into the ZnO NAs, which could enlarge the interfacial area between ETL and active layer.

The photo-electricity of ZnO nanoparticles and nanoarrays have been studied by photoluminsescence (PL) as shown in **Figure 4**, and all samples display two emissions, one sharp emission at about 380 nm for near band edge (NBE), and the other broader one at 450-550 nm for deep level emission (DLE). However, ZnO NAs present a high concentration of surface defeats at 450-550 nm, which could be passivated by introducing an environment-friendly narrow-band gap Ag_2S shell. The PL spectrum of ZA NAs displays similar emission profiles to ZnO NAs in the range from 350 to 600 nm. Upon depositing Ag_2S, the Ag^+ cations and S^{2-} anions in solution will occupy zinc (Zn) vacancies and oxygen (O) vacancies. The Ag^+ and S^{2-} ions provide original nucleation for surface growth of Ag_2S, which can reduce the surface defeats on ZnO NAs correlating with the reduced DLE of PL. The current density-voltage (*J-V*) curves under illuminated of inverted devices employed ZA NAs

with different ZnO NAs thickness as ETL with the architecture of ITO/ETL/P3HT:$PC_{61}BM$/MoO_3/Ag are shown in **Figure S3**, and the corresponding parameters of the devices are listed in **Table S1**. It is obviously that the relative PCE of devices based on ZA NAs with different ZnO NAs thickness are all low. Due to the mismatched energy level between Ag_2S and active layer, the V_{oc} (0.1-0.2 V) is extreme low (**Figure S4**). To improve the energy level alignment, reduce the surface defects of ZnO NAs and increase compatibility between organic active layer and inorganic ETL, CdS QDs shell and solution processed EEMC sensitizing ZnO NAs with different thickness were applied as electron acceptor and ETL of devices simultaneously in PSCs have been studied. The application of QDs and multiple shells could well increase the reflection of light at the interface of ZnO NAs and promote the light absorption.[47]

Figure 5 shows the steady-state *J-V* characteristics of devices based on ZnO NAs, ZnO NAs/EEMC, ZC NAs/EEMC with different thickness ETLs, and **Table 2** reveals the entire photovoltaic performance of these devices. With the addition of EEMC, the PCE of device with ZnO NAs/PTB7:$PC_{71}BM$ initially increases from 6.4% to 6.8%, and the J_{sc} enhances from 15.13 mA/cm^2 to 15.35 mA/cm^2, which is attributed to the good interfacial compatibility between the organic active layer and inorganic and less defects of ZnO after disposition of the EEMC on ZnO nanoarrays. When adopted ZnO NAs (60 nm) sensitized by CdS shell and EEMC as ETL, the J_{sc} of device improves to 17.65 mA/cm^2, resulting in a higher PCE of 7.6%. Meanwhile, the PCE and J_{sc} exhibit a rapid decrease while extending the hydrolysis time, and the tendency are well in accordance with the former results as shown in **Table 1**. In order to combine the advantages of CdS, Ag_2S and EEMC, ZnO NAs of different thickness

sensitized with CdS/Ag_2S double-shells/EEMC are used as ETL to improve the performance of devices based on PTB7:$PC_{71}BM$. As shown in **Figure 6** and **Table 3**, the J_{sc} of devices with ZCA NAs ETL increase slightly by comparing to those of devices based on ZC NAs ETL (in **Table 2**)**.** As shown in **Figure 6**, the energy level of ZC NAs/EEMC and ZCA NAs/EEMC are suitable for devices. Excitingly, the representative ZCA NAs (60 nm)/EEMC device achieves the highest device performance (PCE=7.7%, V_{oc}=0.70 V, J_{sc}=17.90 mA/cm^2, FF=61.4%) under AM 1.5 illuminsation (100 mW/cm^2). Compared to ZnO NPs, the external quantum efficiency (EQE) of the solar cells based on ZnO NAs (in **Figure 6**) increases at around 380 nm, and the corresponding calculated J_{sc} all improve, which are consistent with the value obtained from *J-V* curve. More remarkable, EQE boosts significantly with addition of the quantum dots and EEMC, which due to the optical grating effect leading to increasing the light absorption (incident and back-reflected light)[50] and EEMC assisting the infiltration of active layer into inorganic nanoarrays to obviously improve the compatibility between the two and reduce the charges recombination.

Besides that, the quantum dots have been reported to produce at least two or more electron-hole pairs when absorption of a photon,[50] and to further explore the effect of the quantum dots, so the electron transport characteristics of ZnO NPs/EEMC, ZnO NAs/EEMC, ZA NAs/EEMC, ZC NAs/EEMC and ZCA NAs/EEMC were measured by the space charge limited current (SCLC), and the detailed measurement is showed in **Supporting Information**. The homologous electron-only devices with the structure of ITO/ETL/P3HT:$PC_{61}BM$/LiF/Al is revealed in **Figure 7**. As shown in **Table S2**, due to the higher electrical conductivity of ZnO NAs, CdS and Ag_2S than ZnO NPs, the device with ZCA NAs/EEMC demonstrates the highest electron

mobility of 1.95×10^{-3} cm^2 V^{-1} s^{-1}, while the device with bare ZnO NPs/EEMC reached the lowest electron mobility of 8.98×10^{-4} cm^2 V^{-1} s^{-1}. It further proved that the addition of QDs could enhance electrical conductivity of ZnO NAs.

XPS measurement has been carried out to gain insight into the composition of ZnO NAs with different shells. **Figure 7** shows core level XPS spectra of Zn 2p and O 1s for ZnO NAs, ZC NAs, ZA NAs and ZCA NAs. During the deposition process, the Cd^{2+} and Ag^{+} cations in solution took up Zn vacancies,[51] and S^{2-} anions in solution were readily captured by oxygen vacancies due to the analogous chemical properties of oxygen and sulfur atoms. The captured ions offered the initial nucleation for surface growth of the quantum dots shells, which would result in reduced surface defects of oxygen and Zn vacancies. For ZnO NAs, the binding energy of Zn $2p_{3/2}$ peak is at 1021.7 eV. The maximum of Zn $2p_{3/2}$ peak shifts toward lower binding energy by 0.2 eV as adding the QDs shells onto ZnO NAs, which indicates that more Zn atoms are bounded to oxygen atoms.[5] The O1s XPS spectra demonstrate two peaks with non-symmetricalline shape. One peak with lower binding energy (530.0 eV) corresponds to O atoms in ZnO structure, and the higher peak at 531.5 eV is assigned to an oxygen-deficiency component, such as O1s in $Zn(OH)_2$, or the oxygen species adsorbed by the surface hydroxyl groups.[52, 53] The intensity of the peak at 531.5 eV for all the modified ZnO samples, especially for ZCA NAs, is lower than that of pristine ZnO NAs. It indicates that adding QDs shells onto ZnO NAs avail to reduce the oxygen-deficient component and increase the number of Zn-O bonds in all samples, significantly for CdS/Ag_2S multiple shells. In that case, the separation of charge is increased and the recombination of electron-hole pairs is reduced, which could enhance the performance of devices.

Conclusions

ZnO/Ag_2S, ZnO/CdS core/shell nanoarrays and ZnO/CdS/Ag_2S core/double-shells nanoarrays via environment-friendly hydrolysis reaction as electron transport layers have been successfully applied to improve the photocurrent of PSCs. Ag_2S, CdS shell and CdS/Ag_2S double-shells utilized to passivate deep level defects of ZnO NAs, which could significantly enhance the transport of photogenerated charges and the light absorption. Moreover, solution processed fullerenes (EEMC) was applied to increase compatibility between organic active layer and inorganic electron transport layer. The sensitization of CdS, Ag_2S and EEMC could reduce the defects, increase the electron transportation, and improve light absorption. As a result, the performance of the optimized device with ZC NAs (60 nm)/EEMC was effectively raised to 17.65 mA/cm^2 of J_{sc}, 0.72 V of V_{oc}, 59.8% of FF and 7.6% of PCE. The results imply that inorganic core/shell and core/double-shells nanoarrays is applicable for optimizing device performance as electron transport layer with the advantages of low-cost, environment-friendly and large-scale production.

Acknowledgements

The financial supports for this work are provided by the National Natural Science Foundation of China (51273088 and 51302130) and Doctoral Programs Foundation of Minsistry of Education of China (Grants 20133601110004 and 20133601120006).

Supporting Information

The detailed experimental section; characterizations of the work; space-charge-limited-current (SCLC) mobility measurement of ZnO NAs with

different shells; the synthetic process and ^{1}HNMR figure of EEMC; XRD patterns of ZnO NAs with different thickness of Ag_2S shells; *J-V* curves of ZA NAs; the energy band diagram of glass/ITO/ZA NAs/P3HT:$PC_{61}BM$/MoO_3/Ag solar cell. This information is available free of charge via the Internet at http://pubs.rsc.org/.

References

1. R. Po, C. Carbonera, A. Bernardi and N. Camaioni, *Energy Environ. Sci.*, 2011, **4**, 285.
2. C. E. Small, S. Chen, J. Subbiah, C. M. Amb, S.-W. Tsang, T.-H. Lai, J. R. Reynolds and F. So, *Nat. Photonics*, 2012, **6**, 115.
3. Z. He, C. Zhong, S. Su, M. Xu, H. Wu and Y. Cao, *Nat. Photonics*, 2012, **6**, 591.
4. Y. Liang, Z. Xu, J. Xia, S. T. Tsai, Y. Wu, G. Li, C. Ray and L. Yu, *Adv. Mater.*, 2010, **22**, E135.
5. Y. Sun, J. H. Seo, C. J. Takacs, J. Seifter and A. J. Heeger, *Adv. Mater.*, 2011, **23**, 1679.
6. R. R. Søndergaard, M. Hösel and F. C. Krebs, *J. Polym. Sci. Part B: Polym. Phys.*, 2013, **51**, 16.
7. F. C. Krebs, S. A. Gevorgyan and J. Alstrup, *J. Mater. Chem.*, 2009, **19**, 5442.
8. S. Monticone, R. Tufeu and Kanaev, *J. Phys. Chem. B*, 1998, **102**, 2854.
9. S. Sakohara, M. Ishida and M. A. Anderson, *J. Phys. Chem. B*, 1998, **102**, 10169.
10. S. Mahamuni, B. S. Bendre, V. J. Leppert, C. A. Smith, D. Cooke, S. H. Risbud and H. W. H. Lee, *Nanostruct. Mater.*, 1996, **7**, 659.
11. L. Guo, S. Yang, C. Yang, P. Yu, J. Wang, W. Ge and G. K. L. Wong, *Appl. Phys. Lett.*, 2000, **76**, 2901.
12. S. Kim, C. H. Kim, S. K. Lee, J. H. Jeong, J. Lee, S. H. Jin, W. S. Shin, C. E. Song, J. H. Choi and J. R. Jeong, *Chem. Commun.*, 2013, **49**, 6033.
13. D. Bi, F. Wu, W. Yue, Y. Guo, W. Shen, R. Peng, H. Wu, X. Wang and M. Wang, *J. Phys. Chem. C*, 2010, **114**, 13846.
14. W. U. Huynh, J. J. Dittmer and A. P. Alivisatos, *Science*, 2002, **295**, 2425.
15. P. Ravirajan, A. M. Peiró, M. K. Nazeeruddin, M. Graetzel, D. D. C. Bradley, J. R. Durrant and J. Nelson, *J. Phys. Chem. B*, 2006, **110**, 7635.
16. L. E. Greene, M. Law, B. D. Yuhas and P. Yang, *J. Phys. Chem. C*, 2007, **111**, 18451.
17. S. Dowland, T. Lutz, A. Ward, S. P. King, A. Sudlow, M. S. Hill, K. C. Molloy and S. A. Haque, *Adv. Mater.*, 2011, **23**, 2739.
18. Y.-M. Sung, F.-C. Hsu and Y.-F. Chen, *Sol. Energy Mater. Sol. Cells*, 2014, **125**, 239.
19. C. C. Wu, D. S. Wuu, P. R. Lin, T. N. Chen and R. H. Horng, *Cryst. Growth Des.*, 2009, **9**, 4555.

20. J. Wang, P. Liu, X. Fu, Z. Li, W. Han and X. Wang, *Langmuir*, 2008, **25**, 1218.
21. N. S. Pesika, Z. Hu, K. J. Stebe and P. C. Searson, *J. Phys. Chem. B*, 2002, **106**, 6985.
22. M. L. Kahn, M. Monge, V. Collière, F. Senocq, A. Maisonnat and B. Chaudret, *Adv. Funct. Mater.*, 2005, **15**, 458.
23. C. Z. Li, H. L. Yip and A. K. Y. Jen, *J. Mater. Chem.*, 2012, **22**, 4161.
24. C. H. Hsieh, Y. J. Cheng, P. J. Li, C. H. Chen, M. Dubosc, R. M. Liang and C. S. Hsu, *J. Am. Chem. Soc.*, 2010, **132**, 4887.
25. H. Ma, H. L. Yip, F. Huang and A. K. Y. Jen, *Adv. Funct. Mater.*, 2010, **20**, 1371.
26. B. R. Saunders and M. L. Turner, *Adv. Colloid Interface Sci.*, 2008, **138**, 1.
27. B. Atomsa Gonfa, H. Zhao, J. Li, J. Qiu, M. Saidani, S. Zhang, R. Izquierdo, N. Wu, M. A. El Khakani and D. Ma, *Sol. Energy Mater. Sol. Cells*, 2014, **124**, 67.
28. J. M. Luther, M. C. Beard, Q. Song, M. Law, R. J. Ellingson and A. J. Nozik, *Nano. Letters*, 2007, **7**, 1779.
29. J. Jean, S. Chang, P. R. Brown, J. J. Cheng, P. H. Rekemeyer, M. G. Bawendi, S. Gradecak and V. Bulovic, *Adv. Mater.*, 2013, **25**, 2790.
30. W. U. Huynh, J. J. Dittmer and A. P. Alivisatos, *Science*, 2002, **295**, 2425.
31. K. Yuan, L. Chen, F. Li and Y. Chen, *J. Mater. Chem. C*, 2014, **2**, 1018.
32. Q. Cui, C. Liu, F. Wu, W. Yue, Z. Qiu, H. Zhang, F. Gao, W. Shen and M. Wang, *J. Phys. Chem. C*, 2013, **117**, 5626.
33. K. Yan, L. Zhang, J. Qiu, Y. Qiu, Z. Zhu, J. Wang and S. Yang, *J. Am. Chem. Soc.*, 2013, **135**, 9531.
34. M. Grätzel, *Inorg. Chem.*, 2005, **44**, 6841.
35. Y. Xu and M. A. A. Schoonen, *Am. Mineral.*, 2000, **85**, 543.
36. Y. Lei, H. Jia, W. He, Y. Zhang, L. Mi, H. Hou, G. Zhu and Z. Zheng, *J. Am. Chem. Soc.*, 2012, **134**, 17392.
37. G. Wang, X. Yang, F. Qian, J. Z. Zhang and Y. Li, *Nano Letters*, 2010, **10**, 1088.
38. W.-T. Sun, Y. Yu, H.-Y. Pan, X.-F. Gao, Q. Chen and L.-M. Peng, *J. Am. Chem. Soc.*, 2008, **130**, 1124.
39. J. N. Alexander, S. Higashiya, D. Caskey, H. Efstathiadis and P. Haldar, *Sol. Energy Mater. Sol. Cells*, 2014, **125**, 47.
40. Y. Chen, L. Hu, L. Chen and X. Hu, *J. Mater. Chem. C*, 2014(DOI:10.1039/C4TC01747A).
41. P. Li, X. Li, C. Sun, G. Wang, J. Li, T. Jiu and J. Fang, *Sol. Energy Mater. Sol. Cells*, 2014, **126**, 36.
42. Y. Tak, S. J. Hong, J. S. Lee and K. Yong, *J. Mater. Chem.*, 2009, **19**, 5945.
43. R. S. Devan, R. A. Patil, J.-H. Lin and Y.-R. Ma, *Adv. Funct. Mater.*, 2012, **22**, 3326.
44. D. A. R. Barkhouse, R. Debnath, I. J. Kramer, D. Zhitomirsky, A. G. Pattantyus-Abraham, L. Levina, L. Etgar, M. Grätzel and E. H. Sargent, *Adv.*

Mater., 2011, **23**, 3134.

45. T. J. Savenije, J. M. Warman and A. Goossens, *Chem. Phys. Letters*, 1998, **287**, 148.
46. R. H. Friend, G. J. Denton, J. J. M. Halls, N. T. Harrison, A. B. Holmes, A. Köhler, A. Lux, S. C. Moratti, K. Pichler, N. Tessler, K. Towns and H. F. Wittmann, *Solid State Commun.*, 1997, **102**, 249.
47. A. K. Kyaw, D. H. Wang, D. Wynands, J. Zhang, T. Q. Nguyen, G. C. Bazan and A. J. Heeger, *Nano Letters*, 2013, **13**, 3796.
48. B. Conings, L. Baeten, H.-G. Boyen, D. Spoltore, J. D'Haen, L. Grieten, P. Wagner, M. K. Van Bael and J. V. Manca, *J. Phys. Chem. C*, 2011, **115**, 16695.
49. M. Macias-Montero, A. N. Filippin, Z. Saghi, F. J. Aparicio, A. Barranco, J. P. Espinos, F. Frutos, A. R. Gonzalez-Elipe and A. Borras, *Adv. Funct. Mater.*, 2013, **23**, 5981.
50. O. E. Semonin, J. M. Luther, S. Choi, H. Y. Chen, J. Gao, A. J. Nozik and M. C. Beard, *Science*, 2011, **334**, 1530.
51. P. Kundu, P. A. Deshpande, G. Madras and N. Ravishankar, *J. Mater. Chem.*, 2011, **21**, 4209.
52. T. Rakshit, S. P. Mondal, I. Manna and S. K. Ray, *ACS Appl. Mater. Interfaces*, 2012, **4**, 6085.
53. Y. Zhang, G. Du, X. Wang, W. Li, X. Yang, Y. Ma, B. Zhao, H. Yang, D. Liu and S. Yang, *J. Crystal Growth*, 2003, **252**, 180.

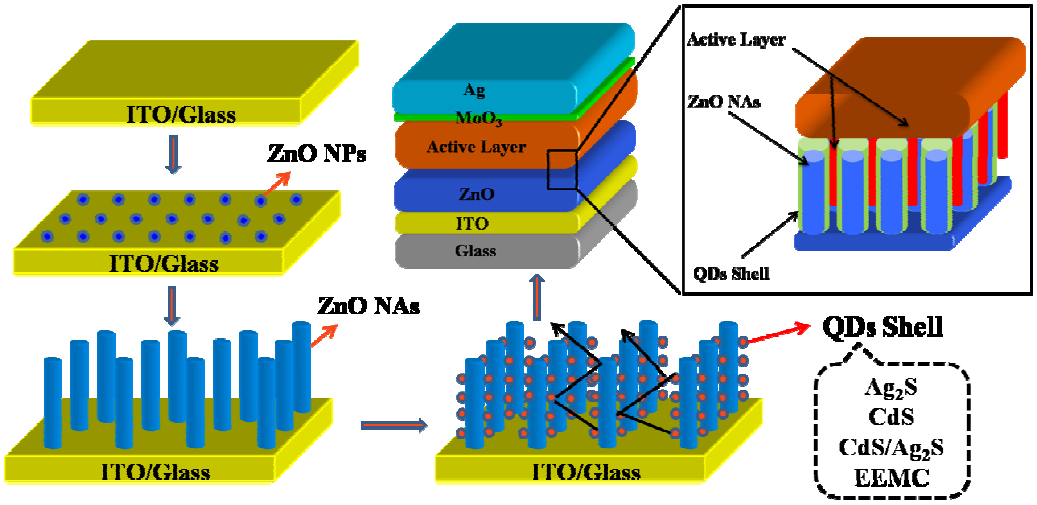

Scheme 1. The preparation of core/double-shells ZnO nanoarrays and the schematic device architecture of the inverted polymer solar cells.

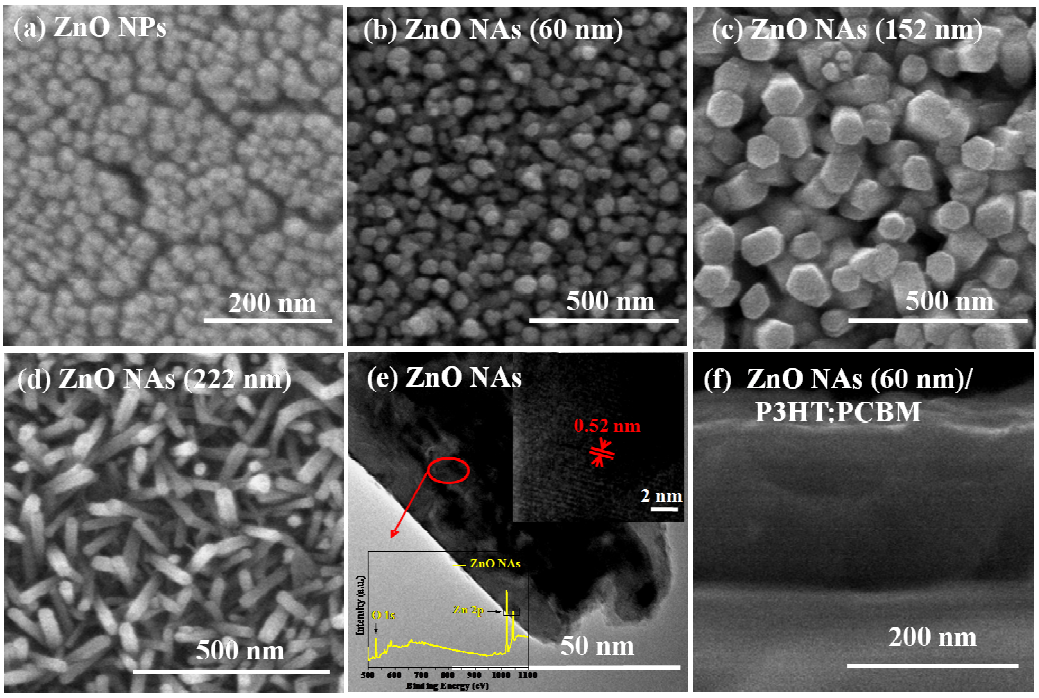

Figure 1. Scanning Electron Microscopy (SEM) images of (a) ZnO NPs, (b, c, d) different thickness of ZnO NAs, (e) TEM image of ZnO NAs and (f) cross-section of ZnO NAs (60 nm)/P3HT:$PC_{61}BM$ with annealing on ITO substrate. The inserts show the XPS and HRTEM of ZnO NAs.

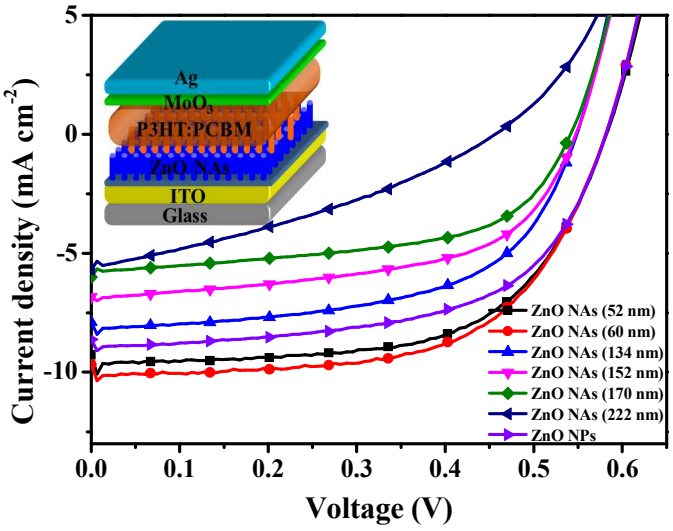

Figure 2. *J-V* curves of devices with different thickness of ZnO NAs (52, 60, 134, 152, 170, 222 nm), and ZnO NPs as electron transport layers for P3HT:$PC_{61}BM$ based solar cells, and the inset of device structure with ZnO NAs as electron transport layer.

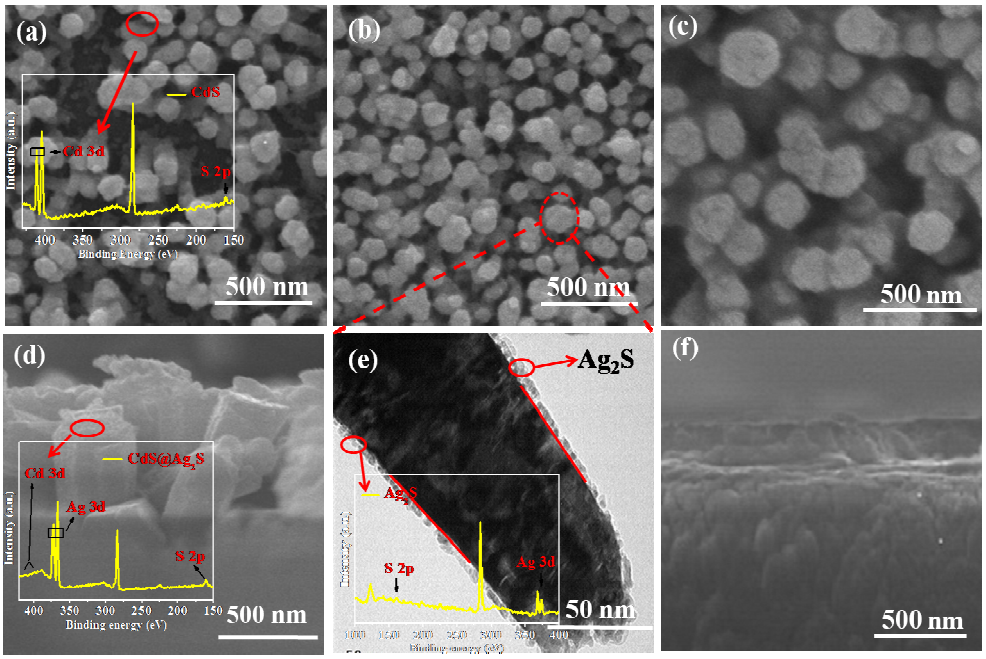

Figure 3. SEM images of (a) ZC NAs, (b) ZA NAs, (c) ZCA NAs, (d) cross-section of ZCA NAs, (e) TEM image of ZA NAs and (f) ZCA NAs/PTB7:$PC_{71}BM$ with annealing. The inserts show the XPS spectra of the corresponding ZnO NAs with different shells.

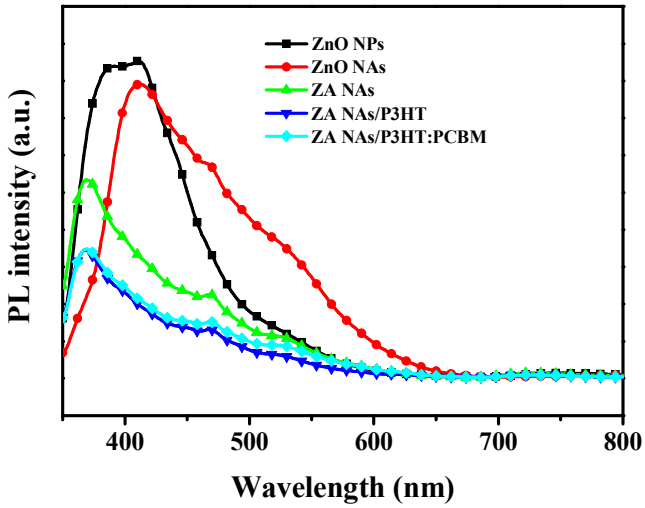

Figure 4. Room temperature PL spectra (excited at 325 nm) of ZnO NPs, ZnO NAs, ZA NAs, ZA NAs/P3HT, and ZA NAs/P3HT:$PC_{61}BM$.

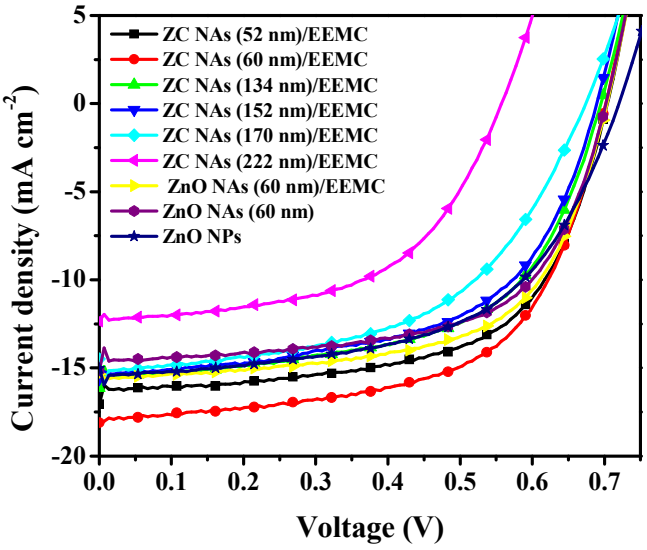

Figure 5. Typical *J-V* curves of devices based on ZnO NAs, ZnO NAs/EEMC, different thickness of ZC NAs/EEMC.

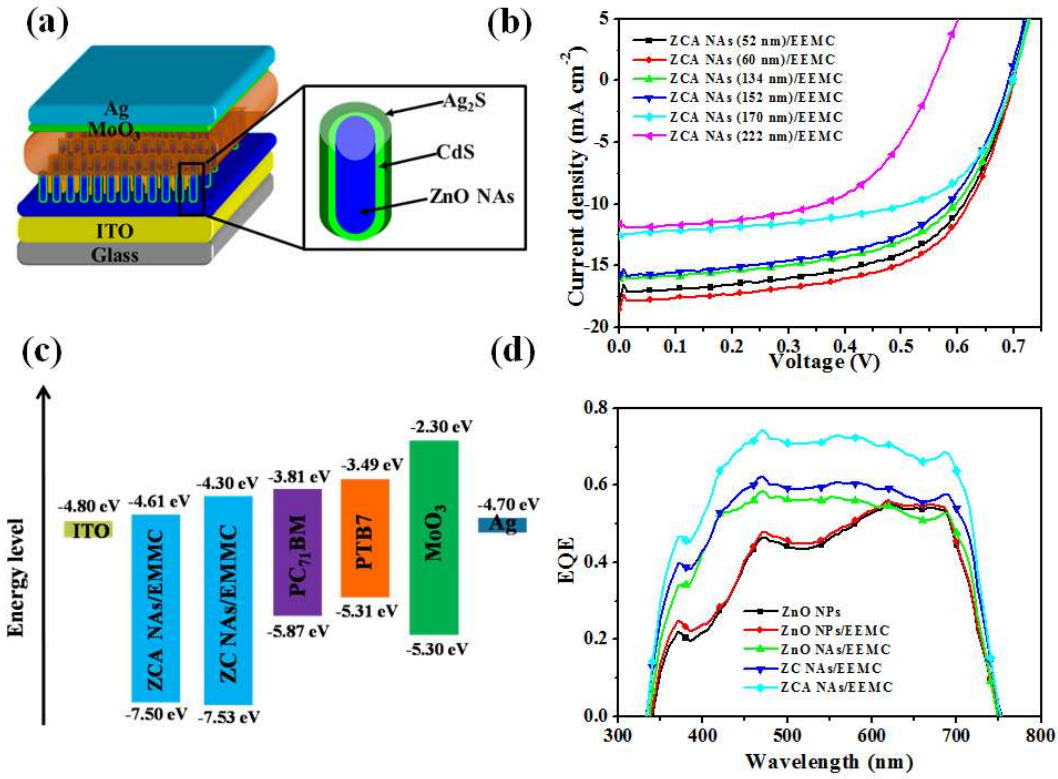

Figure 6. The structure of device based on (a) ZCA NAs/EEMC/PTB7:$PC_{71}BM$, (b) *J-V* curves of devices based on different thickness of ZCA NAs/EEMC/PTB7:$PC_{71}BM$, and (c) the energy level of the related materials used for device fabrication, and (e) EQE spectra of devices with ZnO NPs, ZnO NPs/EEMC, ZnO NAs/EEMC, ZC NAs/EEMC and ZCA NAs/EEMC.

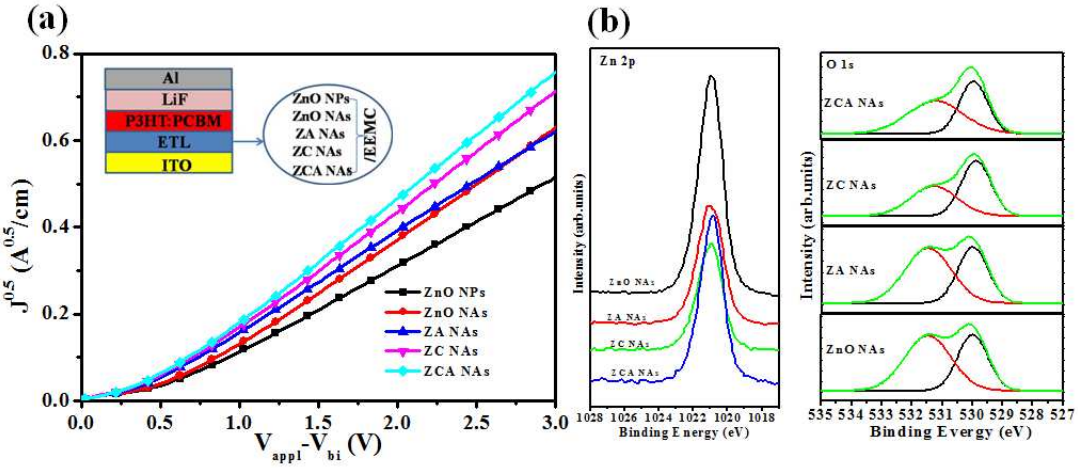

Figure 7. (a) Electron mobilities of ZnO NPs/EEMC or ZnO NAs/EEMC, ZA NAs/EEMC, ZC NAs/EEMC, ZCA NAs/EEMC using the electron-only device measured at ambient temperature. The inset shows the configurations of the electron-only device ITO/ETL/P3HT:$PC_{61}BM$/LiF/Al, (b) XPS spectra of ZnO NAs, ZA NAs, ZC NAs, and ZCA NAs.

Table 1. Device performance of the ZnO NAs/P3HT:$PC_{61}BM$ solar cells under AM 1.5 illuminsation of 100 mW/cm^2.

Hydrolysis time (mins)	Thickness (nm)	J_{sc} (mA·cm^{-2})	V_{oc} (V)	FF (%)	PCE (%)
0	39±5	8.62±0.41	0.58±0.02	60.7±1.7	3.0±0.5(3.5)[a]
10	52±6	9.28±0.42	0.58±0.02	63.6±2.1	3.4±0.3(3.7)[a]
20	60±5	9.68±0.44	0.58±0.02	63.7±1.8	3.6±0.3(3.9)[a]
40	134±8	7.90±0.44	0.55±0.03	59.3±2.2	2.6±0.3(2.9)[a]
60	152±10	6.85±0.55	0.55±0.03	56.6±2.8	2.1±0.3(2.4)[a]
90	170±10	6.00±0.55	0.54±0.03	54.2±2.7	1.8±0.3(2.1)[a]
120	222±10	5.69±0.53	0.45±0.03	32.7±2.1	0.8±0.2(1.0)[a]

[*]All values represent averages from twelve devices on a single chip. [a] The best device PCE.

Table 2. Photovoltaic performance of devices with different ETLs including ZnO NPs, ZnO NAs, ZnO NAs/EEMC and different thickness of ZC NAs/EEMC based on PTB7:$PC_{71}BM$ as active layer.

Device	J_{sc} ($mA \cdot cm^{-2}$)	V_{oc} (V)	FF (%)	PCE (%)
ZnO NPs	15.02±0.45	0.71±0.02	58.1±2.4	6.2±0.5(6.7)[a]
ZnO NAs (60 nm)	15.13±0.48	0.70±0.03	60.2±2.2	6.4±0.6(7.0)[a]
ZnO NAs (60 nm)/EEMC	15.35±0.50	0.70±0.03	62.9±2.2	6.8±0.5(7.3)[a]
ZC NAs (52 nm)/EEMC	17.07±0.55	0.71±0.02	58.5±2.7	7.1±0.4(7.5)[a]
ZC NAs (60 nm)/EEMC	17.65±0.54	0.72±0.02	59.8±2.0	7.6±0.6(8.1)[a]
ZC NAs (134 nm)/EEMC	16.14±0.55	0.70±0.02	56.2±2.6	6.3±0.6(6.9)[a]
ZC NAs (152 nm)/EEMC	15.63±0.54	0.69±0.03	56.2±3.1	6.1±0.7(6.8)[a]
ZC NAs (170 nm)/EEMC	14.50±0.53	0.67±0.03	55.4±3.0	5.4±0.6(6.0)[a]
ZC NAs (222 nm)EEMC	12.34±0.51	0.56±0.05	54.1±2.8	3.7±0.6(4.3)[a]

[*]All values represent averages from twelve devices on a single chip. [a] The best device PCE.

Table 3. Photovoltaic performance of devices with different thickness of ZCA NAs/EEMC/PTB7:$PC_{71}BM$.

Device	J_{sc} ($mA \cdot cm^{-2}$)	V_{oc} (V)	FF (%)	PCE (%)
ZCA NAs (52 nm)/EEMC	17.64±0.54	0.68±0.03	59.0±2.0	7.1±0.5(7.6)[a]
ZCA NAs (60 nm)/EEMC	17.90±0.54	0.70±0.03	61.4±2.1	7.7±0.6(8.3)[a]
ZCA NAs (134 nm)/EEMC	16.38±0.51	0.68±0.03	58.8±1.9	6.6±0.5(7.1)[a]
ZCA NAs (152 nm)/EEMC	15.92±0.53	0.68±0.03	58.1±1.8	6.3±0.5(6.8)[a]
ZCA NAs (170 nm)/EEMC	12.75±0.48	0.67±0.03	59.0±1.8	5.2±0.4(5.6)[a]
ZCA NAs (222 nm)/EEMC	11.64±0.47	0.56±0.05	57.3±2.1	3.7±0.5(4.2)[a]

[*]All values represent averages from twelve devices on a single chip. [a] best device PCE.

Highlights

Tunable Size and Sensitization of ZnO Nanoarrays as Electron Transport Layer for Enhancing Photocurrent of Photovoltaic Devices

Haiyan Fu, Licheng Tan*, Yueqin Shi, Yiwang Chen

Modified ZnO nanoarrays by CdS/Ag_2S double-shells and solution processed fullerenes as electron transport layer realized a PCE of 7.7%.

Graphical abstract